Discrimination and Measurement of Droplet and Ice Crystal by Combining Digital Inline Holography With Interferometric Particle Imaging With Single Color Camera

Yingchun Wu, Xiaoxiang Zhao, Hongyu Zhang, Xiaodan Lin, and Xuecheng Wu

***Abstract*— The discrimination and measurement of complex particle field mixing spherical liquid droplets and other solid irregular particles are challenging but of significance in industry, e.g., droplets and ice crystals in icing wind tunnel or in mixing phase cloud during airplane icing flight test. An approach is proposed by combining digital inline holography (DIH) and interferometric particle imaging (IPI) techniques, and a setup is elaborately designed using a color camera to simultaneously record DIH and IPI signals of the same droplet/ice crystal in the red and green channels of an red-green-blue (RGB) image, respectively. Water droplets and ice crystals generated in a cooling chamber are experimentally tested. The results show that IPI signals tune from regular interferometric fringes to random speckles as water droplet converts into ice crystal, and it is an obvious and robust indicator to discriminate water droplet and ice crystal. Water droplet sizes in the range from 100 to 300 μm measured by DIH and IPI coincide with each other, with relative deviations within ±5%. Concerning ice crystal, the 2-D Fourier transform of IPI speckle pattern agrees well in both overall shape and size with 2-D autocorrelation of DIH reconstructed in-focus image, with size discrepancy within 10%. With the capability of phase discrimination and size and shape measurement, the proposed method combining DIH and IPI has the potential to be instrumented and applied to cloud particle fields.**

***Index Terms*— Droplet, holography, ice crystal, interferometric particle imaging (IPI), shape, size.**

I. Introduction

DROPLETS and ice crystals are two common forms existing in the atmosphere, and they can turn into each other through solidification or melting [1]. Water droplets and ice crystal play a vital role in various applications, e.g., weather prediction and aircraft icing [2]. Water droplet and ice crystals collide with the surface of the aircraft during flight, forming ice on and around the collision area [3]. This kind of icing phenomenon is quite common and poses severe potential dangers to the safety of aircraft, even leading to airplane crash [4]. In view of the adverse effect of icing on aircraft operation, quantitative measurements of water droplet and ice crystal are of practical significance. An implying challenge in this problem is to discriminate water droplet and ice crystal in their coexistences, and a few attempts have been devoted to this problem [5]. Therefore, developments of techniques and instruments for cloud water droplets and ice crystals' discrimination and measurement are of great demand. The community of aviation industry has devoted to water droplet and ice crystal measurement for decades. Thus, different optical techniques have been proposed to measure droplets and ice crystals [6], including light scattering methods, digital holographic imaging, and interferometric particle imaging (IPI) methods. Light scattering methods measure the cloud particle size by collecting the light scattered by particle around a proper angle with a prior knowledge or assumption of particle refractive index. Several instruments have been developed in the framework of this principle, e.g., commercial available phase Doppler particle analyzer (PDPA) which is also called phase Doppler interferometry (PDI) [7], forward scattering spectrometer probe (FSSP) [8], optical array probe (OAP) [9], cloud droplet probe (CDP) [10], airborne droplets analyzer (ADA) [11], and airborne laser interferometric drop sizer (ALIDS) [12], and they have been applied to a variety of icing wind tunnels and flight tests. For instance, in the icing research tunnel in NASA's Glenn Research Center, the mean volume diameter (MVD) of cloud particles was measured with FSSP, OAP, and CDP, with the approximate range of fluctuation and the error obtained [13]–[15]. In the icing wind tunnel in Italy, PDPA, OAP, and ADA measured the MVD and size distribution [16]–[18]. Yet, these techniques are not designed to discriminate and characterize water droplets and ice crystals.

Digital holography records the wavefront complex amplitude of the object light in the form of its interference patterns with the reference wave as hologram and restores the 3-D information of the object via numerical reconstruction. With the capability of retrieving particle size, morphology, and 3-D position, particle holography has been proven to be a powerful tool in the diagnostics of various micrometer-sized particles,

Manuscript received 31 August 2021; revised 3 January 2022; accepted 5 January 2022. Date of publication 14 February 2022; date of current version 12 July 2022. This work was supported in part by the National Natural Science Foundation of China under Grant 52006193, in part by the Zhejiang Provincial Natural Science Foundation of China under Grant LQ19E060010, in part by the National Science and Technology Major Project under Grant 2017-V-0016-0069, and in part by the Open Fund of Key Laboratory of Icing and Anti/De-Icing under Grant AIADL20190103. The Associate Editor coordinating the review process was Dr. Zheng Liu. *(Corresponding author: Yingchun Wu.)*

The authors are with the State Key Laboratory of Clean Energy Utilization, Zhejiang University, Hangzhou 310027, China (e-mail: wycgsp@zju.edu.cn).

Digital Object Identifier 10.1109/TIM.2022.3147333

including pulverized coal particles, droplets in sprays, bubbles, and even burning metal particles [19]. Digital holography has also been applied to cloud particle measurement. An instrument called HoloDec detector via digital in-line holographic imaging with a resolution down to 5 μm was developed [20] and was carried on a C-130 airplane to determine particle size, 2-D shape, and 3-D position in cloud. Beck *et al.* [21] measured both the liquid and ice phase of cloud particle in a liquid cloud and a mixed-phase cloud at the Eggishorn in the Swiss Alps using the HoloGondel platform, and recently, Touloupas *et al.* [22] tempted to identify ice crystals in field measurement data with homemade holographic imager for microscopic objects (HOLIMO) using convolutional neural network. Kaikkonen *et al.* [23] developed an optical cloud droplet and ice crystal measurement system icing condition evaluation method (ICEMET) to measure the droplet size distribution (DSD) and the liquid water content (LWC) of the air. Yet, it is difficult to distinguish water droplets and ice crystals via their projected images, especially when the size reduces to several pixels or the ice crystal is quasi-spherical [24]. One solution to this problem resorts to light scattering patterns. It was found that the polarization of the backward light scattering from small water droplet differs from that of ice crystal and could be used as identification indicator [25]. Light scattering experiments on single ice crystals and droplet revealed that the light scattering patterns by irregular ice crystal are random speckles while the later one are regular fringes well-predicted by Lorenz–Mie scattering, and thus the out-of-focus IPI can be used to discriminate the droplet and ice crystals [26], and even drop-ice mixture. In IPI, the scattered light from the reflection and refraction of the particle interferes at the out-of-focus plane, and the spatial frequency of the fringes/speckles relates to the distance of the reflection refraction glare points and can be eventually used to retrieve the particle size [27]. Yet, the morphology and size measurement accuracy of IPI in ice crystal are not often quantified.

In this work, digital inline holography (DIH) and IPI are combined together to characterize the same droplet/ice crystal, with a hologram and interferogram captured by one color camera. For DIH, through the reconstructed ice crystal in-focus image, we may observe the shape of ice crystal more effectively. For IPI, it is an efficient visual method for the discrimination of droplets and ice crystals, especially when the droplets have just turned into ice crystals or the size of ice crystals is only about several pixels. The out-of-focus IPI can help us discriminate droplets and ice crystals more clearly. Therefore, both the methods have an active effect for this research and the combination is appropriate and essential. Below is the detailed presentation of the experimental setup, data processing, and results.

II. Methodology

A. Experimental Setup and Modeling

The experimental configuration included an optical measurement subsystem which combined a DIH subsystem with an IPI subsystem to characterize droplet and ice crystal in a cooling chamber similar to the one in Kielar *et al.*'s [5] research, as sketched in Fig. 1. In the cooling chamber system, anhydrous ethanol was cooled by an air-cooled refrigerator and pumped into the heat exchange pipe in the cooling chamber. The center hole of the chamber had a diameter of 100 mm and a height of 1000 mm. The chamber can be refrigerated down to −40 °C. The droplets produced by a droplet-on-demand atomizer with size range of 100–300 μm entered the chamber from a small hole at the top, and then was cooled down as falling, eventually reached the measurement section at the bottom and was measured by DIH and IPI. Considering the nucleation process of ice formation, tap water was used in the experiments. The chamber temperature and initial water temperature can be adjusted to provide an environment for liquid droplet and ice phase control in the measurement area.

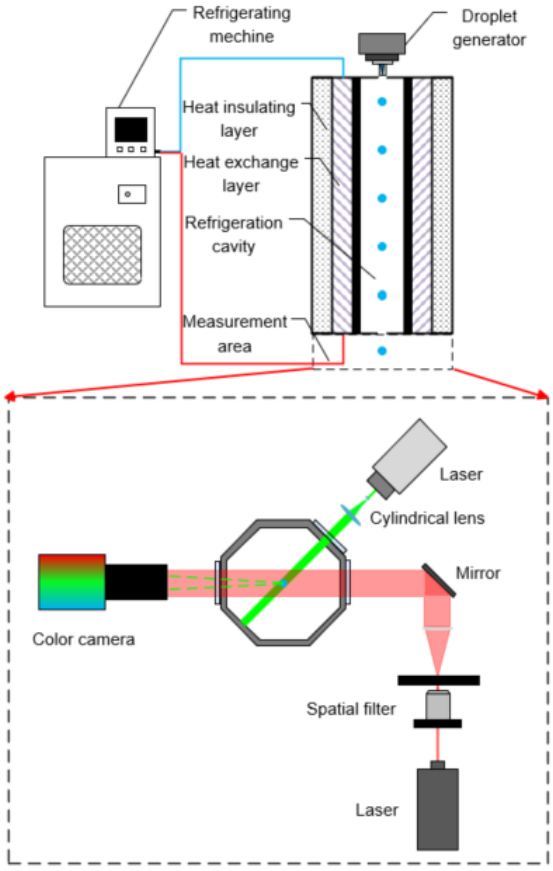

Fig. 1. Experimental setup for water droplets and ice crystals' discrimination and measurement by combining DIH with IPI.

In the measurement section, three K9 optical windows of different angles were installed for DIH and IPI, as illustrated in Fig. 1. In DIH, a continuous He–Ne laser beam with a wavelength of 632.8 nm was used as the light source. The laser beam was expanded by a spatial filter composed of an objective and a pinhole, and then collimated by a convex lens into a plane wave with a diameter of about 50 mm. The parallel laser beam entered the cooling chamber through a K9 optical window to illuminate the droplets and ice crystal particles. When the collimated laser beam illuminates the studied droplet/ice crystal, the light scattered by the droplet/ice

crystal is called the object light, and the light undisturbed by the particle is used as the reference light. The object light and the reference light interfere with each other to form a hologram and the interference fringe intensity of a hologram can be expressed as

$$\mathbf{I}_{\mathrm{H}} = |\mathbf{I}_{\mathrm{O}} + \mathbf{I}_{\mathrm{R}}|^2 = |\mathbf{I}_{\mathrm{O}}|^2 + |\mathbf{I}_{\mathrm{R}}|^2 + \mathbf{I}_{\mathrm{O}}\mathbf{I}_{\mathrm{R}}^* + \mathbf{I}_{\mathrm{O}}^*\mathbf{I}_{\mathrm{R}} \quad (1)$$

where $\mathbf{I}$ is the intensity of the hologram, the subscripts "H, O, and R," respectively, represent "hologram, object light, and reference light," and the symbol * denotes conjugation. The hologram was recorded by a color camera (Basler acA2040-90uc, 2046 × 2040 pixels, 5.5 μm^2/pixel × 5.5 μm^2/pixel) operated at 50 frames/s with an exposure time of 80 μs. A camera lens (Nikon AF 50 mm, 1:1.4D) with an extension tube was inversely mounted to the camera to adjust the magnification of the hologram. The color camera had three recording channels, corresponding to the red, green, and blue channels, with spectral response peaks at 610, 532, and 460 nm, respectively. In this experiment, the hologram of 632.8-nm wavelength was mainly recorded in the red channel.

The same droplet/ice crystal was measured by the IPI system simultaneously. Another continuous diode laser with a wavelength of 532 nm and a maximum power of 2.5 W was used as the light source for IPI. The laser beam was transformed into a laser sheet through a lens group composed of two cylindrical lenses, with a thickness of about 1 mm. Then the laser sheet entered the cooling chamber through a K9 optical window at an angle of 68° to the 632.8-nm holographic beam. The light scattered by the droplet and ice crystal from the 532-nm laser sheet was collected by the same color camera as for the DIH system. The IPI signals were mainly recorded in the green channels. In IPI, when the laser beam illuminates the spherical droplet, the reflected light on the surface of the droplet and the refracted light after passing through the droplet produce two glare points on the infocus image of the droplet, which are attributed to the reflected light and the refracted light, respectively. On the defocused image plane of the droplet, the refracted light and the reflected light interfere with each other to form an interference fringe pattern. Therefore, the defocused interference image of a droplet can be regarded as an interference fringe pattern produced by two glare points. The distance between these two glare points can be obtained using a geometric optics approximation [28]

$$\delta = d/2\left(\cos(\theta/2) + \frac{m\sin(\theta/2)}{\sqrt{m^2 - 2m\cos(\theta/2) + 1}}\right) \quad (2)$$

where d is the diameter of the droplet, θ is the scattering angle of the laser beam, and m is the refractive index of the droplet.

The DIH and IPI systems share a common imaging lens and camera but their signals are separated into different channels, and this design ensures an intrinsic synchronization of the two systems in recording the same particle during camera exposure. There are several experimental tricks in the combination of both the techniques. First, the intensities of the laser beams for DIH and IPI should be adjusted, to ensure the DIH signal in the red channel and the IPI signal in the green channel comparable. Second, the defocus distance and magnification

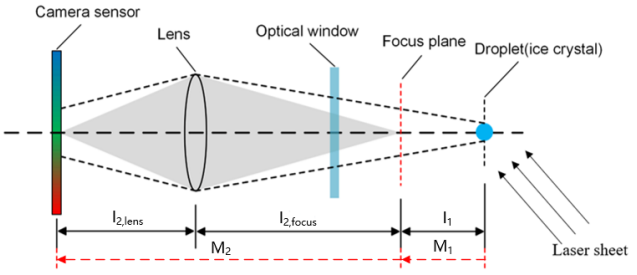

Fig. 2. Schematic of the optical transfer matrix of the IPI experimental system.

TABLE I
EXPERIMENTAL SETTING PARAMETERS

Experiment number	Transverse magnification	Center distance(mm)
1	0.82	35
2	0.82	41
3	0.88	23
4	0.88	25

should be carefully manipulated to a degree where both the fringes of IPI interferogram and hologram can be resolved and sampled. As shown in Fig. 2, the experimental system can be simply modeled as a single lens system according to the matrix optics theory. For the convenience of calculation, the propagation of reflected light and refracted light in the imaging system is divided into two parts, which are the first part $\mathbf{M}_1$ from the droplet/ice crystal to the focus plane and the second part $\mathbf{M}_2$ from the focus plane to the camera sensor. The first part $\mathbf{M}_1$ matrix is determined by the l_1 distance, which is

$$\mathbf{M}_1 = \begin{bmatrix} 1 & l_1 \\ 0 & 1 \end{bmatrix}. \quad (3)$$

The second part $\mathbf{M}_2$ matrix between the focus plane and the camera sensor can be described as

$$\mathbf{M}_2 = \begin{bmatrix} -m_t & 0 \\ -1/f & -1/m_t \end{bmatrix} \quad (4)$$

where m_t is the absolute value of the transverse magnification of the imaging system, and f is the focal length of the lens. Therefore, the total optical matrix between the camera sensor and the measured plane was

$$\mathbf{M}_{\mathrm{tot}} = \begin{bmatrix} A_{\mathrm{tot}} & B_{\mathrm{tot}} \\ C_{\mathrm{tot}} & D_{\mathrm{tot}} \end{bmatrix} = \mathbf{M}_2\mathbf{M}_1. \quad (5)$$

The right-top element $B_{\mathrm{tot}} = m_t l_1$ requires the transverse magnification of the imaging system m_t and the distance l_1 between the droplet/ice crystal and the focus plane. It is worth mentioning that to obtain a high-quality image, we tried different transverse magnifications m_t and distances l_1 in this experiment, as shown in Table I. The center distance represents the distance from the vertical bisector of the focus plane to the laser sheet. For the four cases, the defocus parameter, B_{tot}, varied from 22.4 to 33.6 mm, to yield different spatial resolutions of the recording system, while other parameters were kept unchanged.

According to matrix optics, the frequency F of the interference fringes in IPI can also be obtained from the distance of

the glare point [5]

$$F = \frac{\delta}{\lambda B_{\text{tot}}} \tag{6}$$

where B_{tot} is the B element of the total optical transfer matrix between the plane of the scattering droplet and the plane where the camera sensor is located.

According to the sampling theorem, the sampling frequency should be greater than twice the highest frequency of the signal. Hence, for a camera sensor with pixel pitch p_{x}, to capture the finest fringes of the interferogram, the sampling frequency f must satisfy the following relationship:

$$f = 1/p_x \geq 2\ F. \tag{7}$$

The sampling constraint in (7) implies the lower and upper boundaries of the fringe frequencies and droplet sizes in IPI, and the measurement range of IPI typically spans about 20–300 μm, smaller than that of DIH which covers from several to thousands of microns, and this work focuses on the supercooled large droplet with size larger than 100 μm.

B. Data Processing

1) DIH Processing: The DIH consists of two steps: hologram recording and numerical reconstruction. Hologram numerical reconstruction is a process of simulating the diffraction of the reference wave illuminating the hologram in a computer to restore the wavefront information of the object. In this experiment, the droplet/ice crystal hologram is reconstructed with a wavelet reconstructed algorithm [29]. A slice image at position z can be reconstructed

$$\begin{aligned}\mathbf{I}(x, y; z) &= 1 - \mathbf{I}_{\text{H}}(x, y) \otimes \psi_z(x, y) \\ &= 1 - \mathbf{I}_{\text{H}}(x, y) \otimes \left\{ \frac{\pi}{\lambda z}\left[\sin\left(\frac{\pi}{\lambda z}\left(x^2 + y^2\right)\right) - M_\psi \right] \right. \\ &\quad \left. \times \exp\left(-\frac{\pi\left(x^2 + y^2\right)}{\lambda z \sigma^2} \right) \right\}\end{aligned} \tag{8}$$

where λ is the wavelength of the illumination beam, $\psi_z(x, y)$ is the corrected wavelet function, and σ is the width factor of the windowing function $\exp(-\pi(x^2 + y^2)/(\lambda z \sigma^2))$, which depends on the frame acquisition characteristics. The zeroing parameter M_ψ makes the average value of $\psi_z(x, y)$ zero, which can be expressed as

$$M_\psi = \frac{\sigma^2}{1 + \sigma^4}. \tag{9}$$

The reconstructed droplet/ice crystal image was then further processed, to retrieve the size, shape, and 3-D position, and more details on the DIH processing algorithm can be found in our previous work [30].

2) IPI Processing: The measurement objects of IPI are divided into uniform spherical particles (droplets) and irregular particles (ice crystals). Combining (2) and (6), the relationship between fringe frequency and droplet size can be obtained. Then let us consider the out-of-focus interference image of ice crystals. When the laser beam illuminates the ice crystals, the irregularity of the ice crystal surface causes scattered light of different speckles, which can be regarded as a collection of multiple emitting glare points. Therefore, the defocused light scattering image of an ice crystal is a speckle-like pattern, which is a superposition of mutual interference among all the emitters. The frequency information of the pattern encodes the distance between emitters and can be obtained by 2-D-Fourier transform for speckle pattern. According to the autocorrelation theory, the 2-D-autocorrelation of the ice crystal shape can estimate the maximum size of particles along a certain direction. The 2-D-autocorrelation of the in-focus shape of the ice crystal can be quantitatively determined by the 2-D Fourier transform of the out-of-focus speckle-like pattern [31]

$$|T F_{2D}[\mathbf{I}](\lambda B_{\text{tot}} u, \lambda B_{\text{tot}} v)| = |A_{2D}[G_0](dx, d\ y)| \tag{10}$$

where $\mathbf{I}$ is the intensity of the out-of-focus image of ice crystal, λB_{tot} is the scale factor on both sides of the equation, (u, v) are the transverse coordinates in the frequency domain, and G_0 is the intensity of the electric field emitted by illuminated ice crystal. The key to obtaining the size information of a droplet or an ice crystal from its IPI out-of-focus image lays in the determination of B_{tot} coefficient.

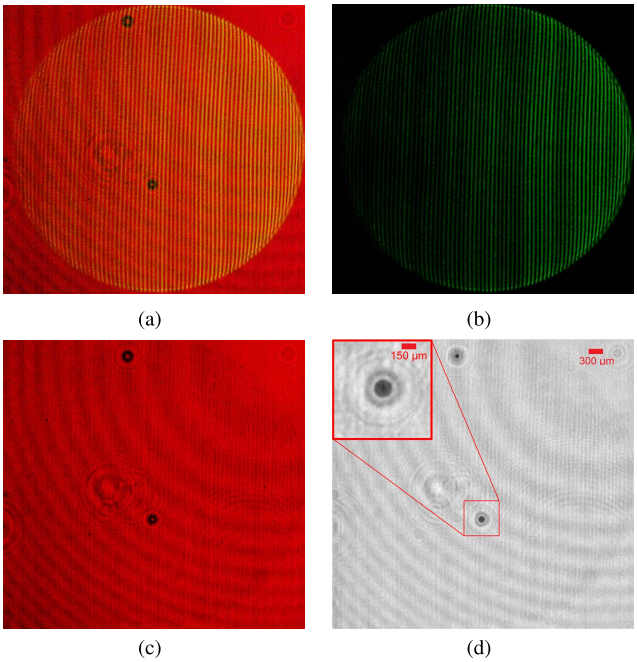

Fig. 3. Experimental results of droplet measured with IPI and DIH. (a) Droplet color interferogram with IPI and DIH signals. (b) Separated IPI signal in the green channel. (c) Separated DIH signal in the red channel. (d) Reconstructed droplet in-focus image from (c).

III. Results and Discussions

A. Droplet Measurement Results

Fig. 3(a) shows a representative experimental interferogram of a droplet captured by the color camera. It is observed that the red DIH reference light signal fills the entire camera plane, in which the holographic fringes are located in the center part. Around the studied droplet, equally spaced green IPI fringes are superimposed on the red hologram. The DIH and

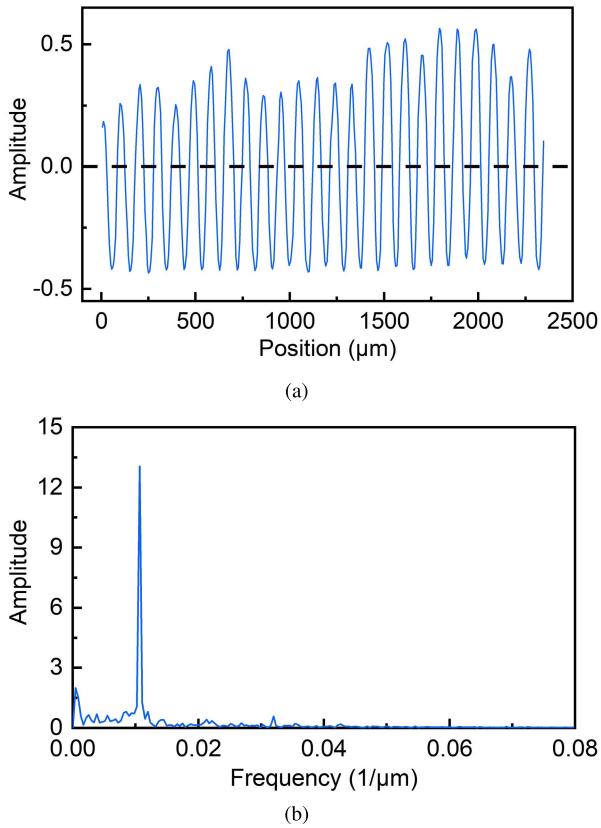

Fig. 4. Processing of IPI signal. (a) Amplitude distribution of IPI signal averaged in the vertical direction in a selected rectangle area. (b) Frequency evaluation of IPI signal with FFT.

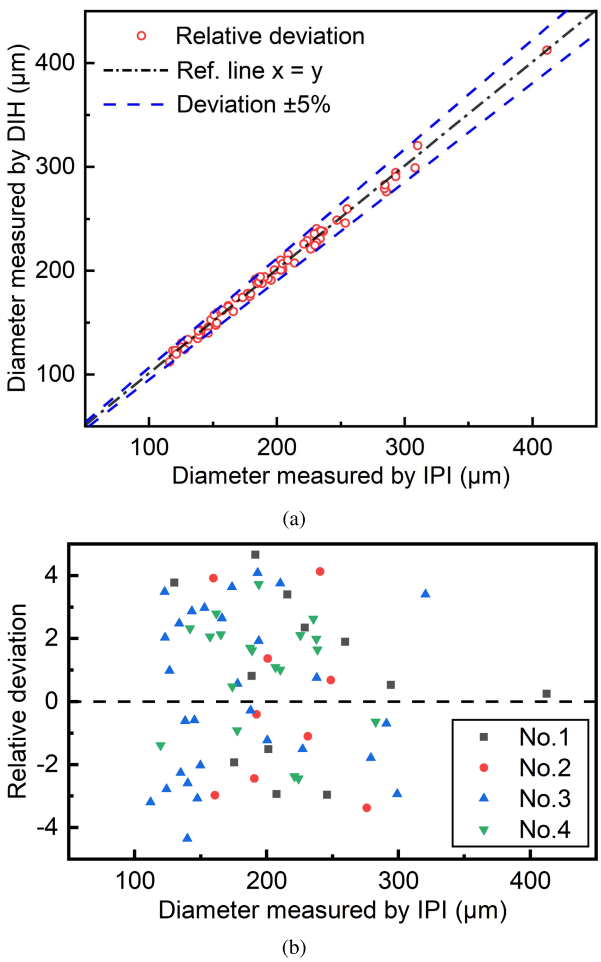

Fig. 5. Comparison of droplet size measurements between IPI and DIH. (a) Droplet size comparison. (b) Relative deviation of diameter measured with IPI compared with DIH.

IPI signals can be separated by extracting the red channel and the green channel of the color image, respectively, as shown in Fig. 3(b) and (c). The crosstalk of the IPI signal into the DIH signal is observed due to the camera's spectral response [32], as evidenced by the weak IPI signal in Fig. 3(c). The superimposed IPI signals do not affect the processing of the DIH since they are in different wavelengths, yet the IPI light intensity should be reduced as much as possible while ensuring the accuracy of the experiment.

The reconstructed in-focus image of the droplet, as shown in Fig. 3(d), is obtained by processing the droplet hologram in Fig. 3(c), with the wavelet reconstruction algorithm. Fig. 3(d) (inset) depicts a zoomed-in view of the target droplet marked with a red rectangle. It can be seen that the droplet has a clear boundary, which is a manifestation of in-focus. This also confirms that the influence of the green light intensity in this experiment on the holographic reconstruction is negligible. The 3-D position of droplet by locating the droplet can also be obtained with DIH [33], and we can match the reconstructed droplets and the IPI signal accordingly. In addition to droplet position, the diameter of the target droplet in Fig. 3(d) is evaluated, with a value of 154 μm.

Then, IPI signal of the same droplet is analyzed as well. The IPI fringes are obtained by averaging a center rectangle region from Fig. 3(b) along the vertical direction. Then, the average amplitude is subtracted to make it concentrated to zero and the amplitude is normalized, as shown in Fig. 4(a). It can be seen that the fringe curve has obvious periodicity. The spatial frequency F of interference fringes can be extracted through fast Fourier transform (FFT), as shown in Fig. 4(b). The results show that the coordinates at dominant frequency peak are (0.01066 μm^{-1}, 13.06). The transverse magnification M_t and the actual defocus distance l_1 are 0.88 and 25.4 mm, respectively. Finally, combining (2) and (6), the diameter of the droplet is calculated to be 157 μm, which generally agrees well with that with DIH (154 μm), with a relative discrepancy of 2.1%.

In this experiment, a total of 69 effective droplets were recorded and analyzed. Fig. 5(a) shows the comparison of size measurement results between DIH and IPI for the same droplets, where the abscissa represents the IPI measurement results, and the ordinate denotes the DIH measurement results. It can be seen that the data points are evenly distributed on both sides of the reference line $y = x$, and the deviations are all within ±5%. Most of the particle size is concentrated between 100 and 300 μm, which is comparable to those of supercooled large droplets. To analyze the deviation of particle size measurement more intuitively, Fig. 5(b) plots the relative deviation of the IPI measurement results compared with DIH and grouped them according to these experimental conditions shown in Table I. In general, the maximum measurement deviation is 4.6%, and the standard deviation is 2.4%. It is

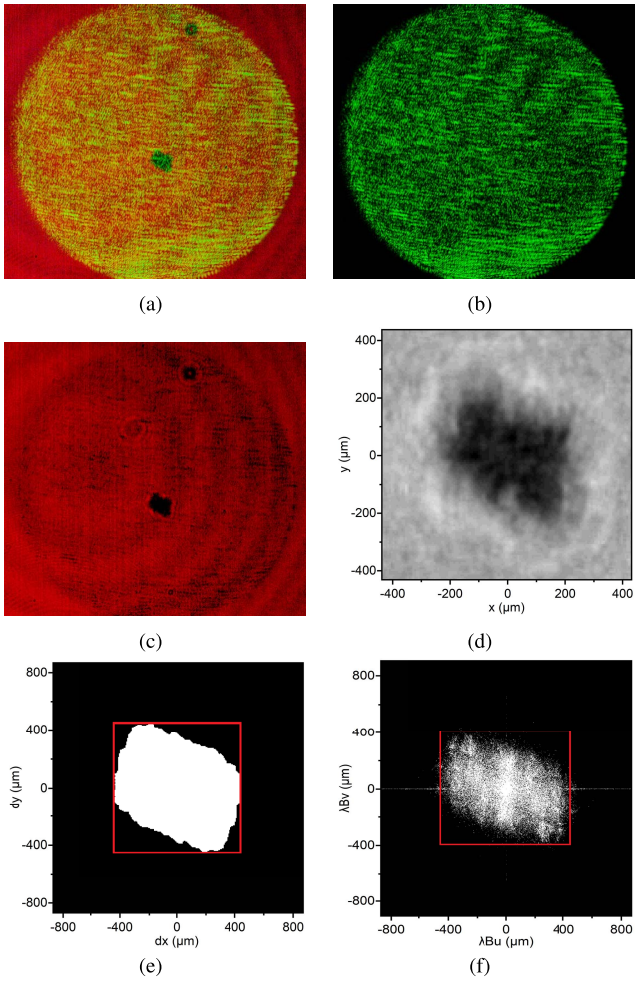

Fig. 6. Experimental results of ice crystal. (a) Ice crystal pictures combined with IPI and DIH. (b) IPI separation image. (c) DIH separation image. (d) Reconstructed ice crystal in-focus image from DIH. (e) Two-dimensional autocorrelation of the ice crystal in-focus image. (f) Binarized 2-D Fourier transform of IPI interferogram.

worth noting that there is no significant change in the relative deviation distribution of particle measurement under different experimental conditions. This proves the reliability of IPI in the measurement of supercooled large droplets.

B. Ice Crystal Measurement Results

Fig. 6(a) shows the experimental interference image of ice crystal. Due to the irregular surface morphology of ice crystal, the defocused interference image of ice crystals is a speckle-like patterns, which substantially differs from regular fringes of water droplet in Fig. 3(a). But the speckle pattern will reduce to regular fringes in the ice crystal which was spherical and fails to discriminate spherical ice crystal from water droplet. The IPI speckle-like pattern of the ice crystal shown in Fig. 6(b) and the ice crystal hologram shown in Fig. 6(c) are obtained by the red-green-blue (RGB) image channel separation. The wavelet reconstruction algorithm shown in (8) is used to reconstruct the ice crystal hologram, yielding the ice crystal in-focus image shown in Fig. 6(d). There was a little fog inside the cooled chamber during droplet icing which deteriorated the hologram and reconstructed image quality a little bit, but the shape and boundary are still clear. The ice crystal image is obtained by binarization of Fig. 6(d),

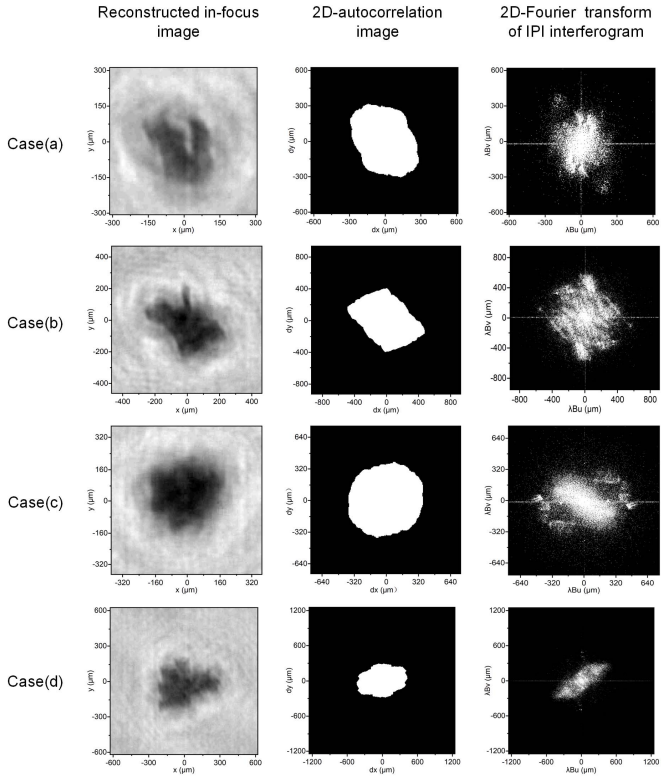

Fig. 7. Data processing results of other four different ice crystals. Case (a)–(d) represent four typical measured ice crystals with various morphology. These three columns are the reconstructed in-focus images, 2D-autocorrelation images and 2D-Fourier transform of IPI interferograms of these ice crystals.

and then the 2-D-autocorrelation is applied in the binary image, yielding Fig. 6(e). According to the 2-D autocorrelation theory, the 2-D autocorrelation of the particle shape reflects the maximum size of the particle along a certain direction, so it is approximately twice the original size of the particle. Concerning IPI, the speckle patterns generated by the light scattering from the ice crystal convey the size information of the ice crystal in the speckle frequency, which can be retrieved by 2-D Fourier transform as shown in Fig. 6(b). Then the 2-D Fourier spectrum of IPI speckle patterns is segmented using an appropriate threshold to obtain a binary image as shown in Fig. 6(f). According to (10), to convert the scale of the 2-D-Fourier spectrum to the real size of the ice crystal particle, the scale of the binary 2-D-Fourier spectrum is adjusted by the scale factor λB_{tot}. Ignoring the discrete points in Fig. 6(f), it can be seen that Fig. 6(e) and (f) have good consistency in shape, and both shapes are overall parallelograms. For further quantitative comparison, the bounding rectangle of the overall shape is measured, with the size of 884 μm $\times$ 891 μm in Fig. 6(e) and 911 μm $\times$ 816 μm in Fig. 6(f), respectively, with deviations within 10%.

To further validate the reliability of the system, more ice crystals are tested with representative results shown in Fig. 7. Four typical ice crystals of different shapes and sizes are selected, and the first, second, and third rows give the in-focus ice crystal image reconstructed from DIH, the autocorrelation of the in-focus image, and the size and shape retrieved from IPI speckle pattern, respectively. From the 2-D-autocorrelation of four typical ice crystals, cases (a) and (b) are similar

to parallelogram, and cases (c) and (d) look like ellipses. As shown in the third column of Fig. 7, all ice crystals have relatively good consistency in shape and size between IPI measurements and DIH measurements. The shape of the image has some discrepancies in the detailed morphologies, and this could be attributed to the thresholding of 2-D Fourier transform. A quantitative comparison of the characteristics lengths in the x and y directions between the second and third columns indicates that the discrepancies are within 4%–10% for the four cases. Note that the IPI speckle pattern enables the retrieving of rough morphology of ice crystal for size measurement, but cannot achieve the fine structure of ice crystal as in DIH, as evidenced in Figs. 6 and 7.

Both the DIH and IPI signals of water droplet and ice crystal have distinguishing features in the discriminating demonstration, as shown in Figs. 3 and 6. Yet it should be pointed that DIH, as a 3-D imaging technique, and IPI, as a light scattering imaging technique, have different strengths in particle measurement and discrimination. Concerning particle position measurement, DIH can acquire the 3-D information of the particles, such as its 3-D spatial position, while IPI usually obtains 2-D transversal position except using special astigmatic configurations [34], [35]. Besides, the particle diameter measurement range of IPI is quite limited (from tens to hundreds of microns), while for DIH, the range can be extended, from to several microns and to even millimeter level. Moreover, DIH can obtain the morphology of relatively large ice crystal accurately. The discrimination of ice crystal and water droplet with DIH is based on the visual effect of reconstructed particle image, and the implication is that the image difference should be no less than one pixel at least, that is, of the order of several microns, and that the droplet/crystal should be large enough (usually occupying over ten pixels). While IPI is sensitive to the morphology irregularity caused by ice crystal of the order of wavelength, that is, down to sub-nanoscale, and thus is more effective in discrimination especially for small droplet/crystal. Thus, the combination of DIH and IPI can provide an approach for both accurate size measurement and effective phase discrimination.

IV. Conclusion

This work investigates a droplet and ice crystal measurement system combining DIH with IPI, by elaborately using a color camera to simultaneously record but separate the interferometric signals from the DIH and IPI of the same droplet/ice crystal. The cooling chamber is used to freeze the falling liquid droplets and generates ice crystals.

1) The simultaneous measurement of the DIH and IPI signals is realized using a color camera and a specific optical path arrangement, ensuring that the same particles are detected from the same projection view. Then, the DIH and IPI signals are separated by the RGB channel separation.
2) The DIH and IPI signals of 69 water droplets are analyzed and compared. The droplet size spans from 100 to 300 μm in the typical supercooled large droplet range, and all the relative deviations in size measurement between DIH and IPI are within $\pm 5\%$.
3) The DIH and IPI signals of five representative shapes of ice crystals are processed and analyzed. The IPI speckle pattern of ice crystal distinguishes from the regular fringes of water droplet, and this can be used to discriminate water droplet and ice crystal. The 2-D Fourier transform of the ice crystal IPI interferogram and the corresponding 2-D autocorrelation of the DIH reconstructed focus image have good consistency in shape and size, with discrepancy within 10%.

DIH performs better in the morphology and size measurement of ice crystals, while IPI shows its superiority on the discrimination of small ice crystals and water droplets. Hence, the collaborate design, which combines the particle light scattering pattern by IPI and particle image by DIH, demonstrates to be an effective tool to identify the phase state of water droplets and ice crystals. Considering the high sensitivity of light scattering pattern on particle shape in IPI, the combination of both the techniques has the potential to discriminate water droplet and ice crystal when the size reduces to several pixels. This setup can be further instrumented to discriminate and measure water droplets and ice crystals in icing wind tunnels and icing flight test of airplanes.

References

[1] B. J. Murray, D. A. Knopf, and A. K. Bertram, "The formation of cubic ice under conditions relevant to Earth's atmosphere," *Nature*, vol. 434, no. 7030, pp. 202–205, Mar. 2005.
[2] Y. Zhao, Q. Guo, T. Lin, and P. Cheng, "A review of recent literature on icing phenomena: Transport mechanisms, their modulations and controls," *Int. J. Heat Mass Transf.*, vol. 159, Oct. 2020, Art. no. 120074.
[3] Y. Cao, Z. Wu, Y. Su, and Z. Xu, "Aircraft flight characteristics in icing conditions," *Prog. Aerosp. Sci.*, vol. 74, pp. 62–80, Apr. 2015.
[4] B. D. et d'Analyses. (2012). *Pour la Sécurité de l'Aviation Civile, Final Report: On the Accident on 1st June 2009 to the Airbus a330–203 Registered F-GZCP Operated by Air France Flight AF 447 Rio de Janeiro-Paris*. [Online]. Available: http://e1.flightcdn.com/live/special/Air_France_447_AFR447_Final_Report-en.pdf
[5] J. J. Kielar, Y. Wu, S. Coëtmellec, D. Lebrun, G. Gréhan, and M. Brunel, "Size determination of mixed liquid and frozen water droplets using interferometric out-of-focus imaging," *J. Quant. Spectrosc. Radiat. Transf.*, vol. 178, pp. 108–116, Jul. 2016.
[6] D. Baumgardner *et al.*, "Airborne instruments to measure atmospheric aerosol particles, clouds and radiation: A cook's tour of mature and emerging technology," *Atmos. Res.*, vol. 102, pp. 10–29, Oct. 2011.
[7] P. Y. Chuang *et al.*, "Airborne phase Doppler interferometry for cloud microphysical measurements," *Aerosol Sci. Technol.*, vol. 42, no. 8, pp. 685–703, Jun. 2008.
[8] J. E. Dye and D. Baumgardner, "Evaluation of the forward scattering spectrometer probe—Part I: Electronic and optical studies," *J. Atmos. Ocean. Technol.*, vol. 1, pp. 329–344, Dec. 1984.
[9] P. R. Field, A. J. Heymsfield, and A. Bansemer, "Shattering and particle interarrival times measured by optical array probes in ice clouds," *J. Atmos. Ocean. Technol.*, vol. 23, no. 10, pp. 1357–1371, Oct. 2006.
[10] S. Lance, C. Brock, D. Rogers, and J. A. Gordon, "Water droplet calibration of the Cloud Droplet Probe (CDP) and in-flight performance in liquid, ice and mixed-phase clouds during ARCPAC," *Atmos. Meas. Techn.*, vol. 3, no. 6, p. 1683, 2010.
[11] T. W. Choularton *et al.*, "The influence of small aerosol particles on the properties of water and ice clouds," *Faraday Discuss.*, vol. 137, pp. 205–222, Jan. 2008.
[12] E. Porcheron *et al.*, "Development of the ALIDS spectrometer for airborne measurement of the droplets size in clouds," in *Proc. 16th Int. Symp. Flow Visualizat.*, 2014, pp. 1–14.
[13] R. Ide and J. Oldenburg, "Icing cloud calibration of the NASA Glenn icing research tunnel," in *Proc. 39th Aerosp. Sci. Meeting Exhib.*, Jan. 2001, p. 234.
[14] J. Van Zante, R. Ide, and L.-C. Steen, "NASA Glenn icing research tunnel: 2012 cloud calibration procedure and results," in *Proc. 4th AIAA Atmos. Space Environ. Conf.*, Jun. 2012, p. 2933.

[15] J. F. VanZante *et al.*, "NASA Glenn icing research tunnel: 2014 cloud calibration," SAE AC-9C Aircr. Icing Technol. Committee Fall Meeting, Tech. Rep. GRC-E-DAA-TN18729, 2014

[16] L. Imperato, G. Leone, and L. Vecchione, "Spray nozzles experiment comparison in laboratory and icing wind tunnel testing," in *Proc. 38th Aerosp. Sci. Meeting Exhib.*, Jan. 2000, p. 487.

[17] M. Bellucci, B. Esposito, M. Marrazzo, G. Fatigati, and F. Ferrigno, "Calibration of the CIRA IWT in the low speed configuration," in *Proc. 45th AIAA Aerosp. Sci. Meeting Exhib.*, Jan. 2007, p. 1092.

[18] B. Esposito and M. Marrazzo, "Application of PDPA system with different optical configuration to the IWT calibration," in *Proc. 45th AIAA Aerosp. Sci. Meeting Exhib.*, Jan. 2007, p. 1094.

[19] J. Katz and J. Sheng, "Applications of holography in fluid mechanics and particle dynamics," *Annu. Rev. Fluid Mech.*, vol. 42, no. 1, pp. 531–555, Jan. 2010.

[20] J. P. Fugal and R. A. Shaw, "Cloud particle size distributions measured with an airborne digital in-line holographic instrument," *Atmos. Meas. Techn.*, vol. 2, no. 1, pp. 259–271, Jun. 2009.

[21] A. Beck, J. Henneberger, S. Schöpfer, J. Fugal, and U. Lohmann, "HoloGondel: *In situ* cloud observations on a cable car in the Swiss Alps using a holographic imager," *Atmos. Meas. Techn.*, vol. 10, no. 2, pp. 459–476, Feb. 2017.

[22] G. Touloupas, A. Lauber, J. Henneberger, A. Beck, and A. Lucchi, "A convolutional neural network for classifying cloud particles recorded by imaging probes," *Atmos. Meas. Techn.*, vol. 13, no. 5, pp. 2219–2239, May 2020.

[23] V. A. Kaikkonen, E. O. Molkoselkä, and A. J. Mäkynen, "A rotating holographic imager for stationary cloud droplet and ice crystal measurements," *Opt. Rev.*, vol. 27, no. 2, pp. 205–216, Apr. 2020, doi: 10.1007/s10043-020-00583-y.

[24] T. Nousiainen and G. M. McFarquhar, "Light scattering by quasi-spherical ice crystals," *J. Atmos. Sci.*, vol. 61, no. 18, pp. 2229–2248, Sep. 2004. [Online]. Available: https://journals.ametsoc.org/view/journals/atsc/61/18/1520-0469_2004_061_2229_lsbqic_2.0.co_2.xml

[25] Z. Ulanowski, E. Hirst, P. H. Kaye, and R. Greenaway, "Retrieving the size of particles with rough and complex surfaces from two-dimensional scattering patterns," *J. Quant. Spectrosc. Radiat. Transf.*, vol. 113, no. 18, pp. 2457–2464, Dec. 2012.

[26] M. Brunel, M. Talbi, S. Coetmellec, G. Grehan, Y. Wu, and J. Jacquot-Kielar, "Interferometric out-of-focus imaging of freezing droplets," *Opt. Commun.*, vol. 433, pp. 173–182, Feb. 2019.

[27] M. Brunel, H. Shen, S. Coëtmellec, G. Gréhan, and T. Delobel, "Determination of the size of irregular particles using interferometric out-of-focus imaging," *Int. J. Opt.*, vol. 2014, pp. 1–8, Jan. 2014.

[28] N. Semidetnov and C. Tropea, "Conversion relationships for multidimensional particle sizing techniques," *Meas. Sci. Technol.*, vol. 15, no. 1, p. 112, 2003.

[29] M. Malek, S. Coëtmellec, D. Allano, and D. Lebrun, "Formulation of in-line holography process by a linear shift invariant system: Application to the measurement of fiber diameter," *Opt. Commun.*, vol. 223, nos. 4–6, pp. 263–271, Aug. 2003.

[30] W. Yingchun *et al.*, "Wavelet-based depth-of-field extension, accurate autofocusing, and particle pairing for digital inline particle holography," *Appl. Opt.*, vol. 53, no. 4, pp. 556–564, 2014.

[31] M. Brunel, S. G. Ruiz, J. Jacquot, and J. van Beeck, "On the morphology of irregular rough particles from the analysis of speckle-like interferometric out-of-focus images," *Opt. Commun.*, vol. 338, pp. 193–198, Mar. 2015.

[32] Y. Wu, Z. Lin, X. Wu, and K. Cen, "Dual-beam interferometric particle imaging for size measurement of opaque metal droplet," *Powder Technol.*, vol. 356, pp. 31–38, Nov. 2019.

[33] X. Wu *et al.*, "Dual-beam interferometric particle imaging for size and shape characterization of irregular coal micro-particle: Validation with digital inline holography," *J. Quant. Spectrosc. Radiat. Transf.*, vol. 241, Jan. 2020, Art. no. 106728.

[34] H. Shen, S. Coetmellec, and M. Brunel, "Cylindrical interferometric out-of-focus imaging for the analysis of droplets in a volume," *Opt. Lett.*, vol. 37, no. 19, pp. 3945–3947, 2012.

[35] B. Wen, Y. Wu, Z. Zhuo, and X. Wu, "Characterization and verification of astigmatic interferometric particle imaging for volumetric droplet 3D position and size measurement," *Adv. Powder Technol.*, vol. 32, no. 10, pp. 3476–3483, Oct. 2021. [Online]. Available: https://www.sciencedirect.com/science/article/pii/S0921883121003721

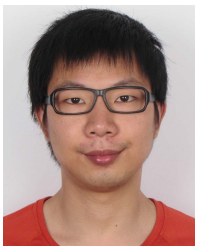

Yingchun Wu received the B.S. degree from the University of Science and Technology of China, Hefei, China, in 2009, and the Ph.D. degree from Zhejiang University, Hangzhou, China, in 2014.

He is currently a Research Professor of the "100 Talents Program" with the College of Energy Engineering, Zhejiang University. He has published over 80 papers in scientific journals and international conferences in related areas. His current research interests include advanced optical measurement techniques, such as holographic imaging 3-D measurement technology, light scattering imaging measurement technology, and laser-induced grating spectroscopy; fuel particle dynamic diagnosis, such as spray atomization, evaporation measurement, combustion diagnosis, and droplet generation; and flow field diagnosis technology.

Xiaoxiang Zhao received the B.S. degree from Zhejiang University, Hangzhou, China, in 2020, where he is currently pursuing the M.S. degree with the College of Energy Engineering.

His current research interests include holographic imaging, particle measurement, droplet icing, and droplet impact.

Hongyu Zhang received the B.S. degree from the Huazhong University of Science and Technology, Wuhan, China, in 2018, and the M.S. degree from Zhejiang University, Hangzhou, China, in 2021.

His current research interests include interferometric imaging, particle measurement, droplet icing, and droplet impact.

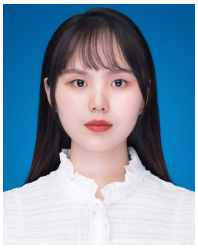

Xiaodan Lin received the B.S. degree from the Huazhong University of Science and Technology, Wuhan, China, in 2016, and the Ph.D. degree from Zhejiang University, Hangzhou, China, in 2021.

Her current research interests include digital holography, coal particle measurement, droplet icing, and droplet impact.

Xuecheng Wu received the B.S. and Ph.D. degrees from Zhejiang University, Hangzhou, China, in 2001 and 2007, respectively.

He is currently a Professor with the College of Energy Engineering, Zhejiang University. He has published over 150 papers in scientific journals and international conferences in related areas. His current research interests include measurement and diagnosis of complex multiphase flow and reaction systems, monitoring and technical evaluation of flue gas pollutants, and operation monitoring and optimization of energy utilization processes.